

Experimental Evaluation of Single-Bolted Lap Joints at Elevated Temperatures

Erica C. Fischer, Ph.D., P.E., M.ASCE¹; Amit H. Varma, Ph.D., Aff.M.ASCE²; and Qiaqia Zhu³

Abstract: In U.S. building construction, typical simple (shear) connections are often bolted for flexibility during fabrication and construction. This paper summarizes the results of experimental investigations of bolted lap-splice joints at elevated temperatures. This paper provides a comprehensive overview of previously tested bolted lap-splice joints at elevated temperatures and a new testing series performed by the authors. Bolted lap-splice joints represent a simple approximation of simple bolted connections. The authors tested specimens using steady-state conditions at targeted temperatures. The tests considered two failure modes: bolt shear fracture and bolt bearing. The authors considered varying parameters within the connection such as bolt diameter, edge distance, and thickness of plate. The results of these experiments are temperature-dependent bolt shear fracture capacities and experimentally measured axial force–deformation–temperature relationships. The temperature-dependent bolt shear fracture capacities are compared with those capacities previously measured by other researchers and the temperature-dependent retention factors provided in Eurocode. The axial force–deformation relationships are compared with previously developed numerical models. DOI: 10.1061/(ASCE)ST.1943-541X.0001911. © 2017 American Society of Civil Engineers.

Author keywords: Fire; Bolted connections; Steel; Metal and composite structures.

Introduction and Motivation

Simple bolted connections are used in steel-frame buildings to connect gravity frame members together. These connections are popular in U.S. building practices because they provide dimensional flexibility during construction and do not require special inspections. Simple bolted connections are designed for vertical shear force only at ambient temperature. However, during a fire, composite floor beams of steel-frame buildings expand during the heating phase of the fire and contract during the cooling phase of the fire. This expansion and contraction imposes large axial forces and moments on the connections. Because these connections are not designed or detailed to resist axial force or moment, these connections are vulnerable to the following failure modes during fire: bolt shear fracture, tearout failure of the plate, and weld rupture. Failure of simple bolted connections within gravity frames can lead to larger unbraced column lengths than designed for. The floor beams of a building brace columns against buckling. When a beam-to-column connection fails, the column's unbraced length increases to two story heights of unbraced length. This behavior can lead to column buckling, partial or full collapse of a building, and spreading of the fire. In order for engineers to simulate the performance of steel-frame buildings during fire and design members and connections for the imposed loads and moments due to fire, they

must have tools to quantify the temperature-dependent behavior of simple bolted connections. This behavior includes the temperature-dependent axial force–deformation (P – δ) behavior.

Previous researchers performed experimental and numerical investigations (Sarraj 2007; Kirby 1995; Rex and Easterling 2003; Yu et al. 2009; Hanus et al. 2011; Hu and Engelhardt 2011; Agarwal et al. 2014; Hirashima et al. 2014; Zhu et al. 2014) to quantify the temperature-dependent axial force capacity of simple bolted connections. Quantifying this capacity is a three-dimensional problem because of the clamping effect caused by the bolts. The capacity also must consider the interaction between the connection components including slip, contact, elastic-plastic deformation, and separation. One method used to simulate the inherent temperature-dependent behavior of bolted simple connections is a series of nonlinear springs. These springs simulate the axial force–deformation–temperature (P – δ – T) relationships for controlling failure modes of the connection, namely bolt shear fracture and plate bearing.

Axial force–deformation (P – δ) relationships were developed by researchers to aid engineers in predicting the behavior of simple connections at elevated temperatures (Block et al. 2007; Sarraj 2007; Agarwal et al. 2014). However, these relationships were developed using the Eurocode 3 (CEN 2005) temperature-dependent material properties and benchmarked against experiments using European-grade steels (Yu et al. 2009).

This paper provides a comprehensive overview of previous experiments performed on lap-splice joints at elevated temperatures followed by a discussion of the lap-splice joint tests performed by the authors. The experiments performed by the authors use U.S.-grade steel typically used in U.S. construction practice. The purpose of these experiments is to understand the applicability of previously developed component models (Sarraj 2007; Agarwal et al. 2014) to U.S. building construction and design practice. This is achieved by comparing the component models (Sarraj 2007; Agarwal et al. 2014) to the experimentally measured axial force–deformation (P – δ) relationships.

¹Assistant Professor, Dept. of Civil and Construction Engineering, Oregon State Univ., 101 Kearney Hall, Corvallis, OR 97330 (corresponding author). E-mail: erica.fischer@oregonstate.edu

²Professor, Robert L. and Terry L. Bowen Laboratory, Lyles School of Civil Engineering, Purdue Univ., West Lafayette, IN 47907. E-mail: ahvarma@purdue.edu

³Engineer, KPFF, 1601 5th Ave. #1600, Seattle, WA 98101. E-mail: qzhu@kpff.com

Note. This manuscript was submitted on January 17, 2017; approved on June 9, 2017; published online on October 31, 2017. Discussion period open until March 31, 2018; separate discussions must be submitted for individual papers. This paper is part of the *Journal of Structural Engineering*, © ASCE, ISSN 0733-9445.

Background

Previous research on simple connections (Kirby 1995; Rex and Easterling 2003; Yu et al. 2009; Hanus et al. 2011; Hu and Engelhardt 2011; Agarwal et al. 2014; Hirashima et al. 2014; Fischer and Varma 2015; Fischer et al. 2016) provides insight into governing failure modes of simple connections subjected to axial force at elevated temperatures and modeling techniques to simulate the performance of bolted simple connections during fire conditions.

Experimental tests on lap-splice joints have also provided insight into temperature-dependent material properties of bolts. ASTM A325 (ASTM 2014c) bolts are commonly used in simple connections in U.S. steel building construction. These bolts are tempered at a temperature of 427°C (ASTM 2014c). Previous research has observed a significant reduction in shear stress (Yu 2006; Hu and Engelhardt 2011; Kodur et al. 2012) when the bolt temperature is greater than 400°C.

Previous Experimental Research

Kirby (1995) tested Grade 8.8 bolts in tension and in double-shear at temperatures up to 800°C to compare temperature-dependent bolt shear and tensile capacities with the existing Eurocode 3 guidelines for fire limit states. Grade 8.8 bolts are widely used throughout Europe in steel-frame building construction; however, temperature-dependent shear stress retention factors of Grade 8.8 bolts are different than ASTM A325 bolts. The tests performed by Kirby demonstrated significant loss in ultimate bolt capacity at 300°C. At temperatures above 700°C the bolts retained limited strength. Retention factors provided in BS5950 (BSCA 2001) were compared with those obtained experimentally and found to be conservative especially in the lower temperature regions.

Rex and Easterling (2003) performed a series of tests to investigate plate bearing behavior of connections at ambient temperature only. Lap-splice joints were loaded in tension to measure the axial force–deformation (P – δ) relationship. Influence of parameters such as plate thickness, edge distance, plate yield stress, plate ultimate stress, and bolt diameter were examined. Rex and Easterling (2003) observed four different types of failure modes from the tests: (1) bearing; (2) tearout; (3) splitting; and (4) curling of the plate. The results of these tests were used to develop a numerical model for the initial stiffness of the axial force–deformation (P – δ) relationship. This numerical model was used as the basis of other numerical models developed by Sarraj (2007) and Agarwal et al. (2014).

Yu et al. (2009) tested a series of bolts in shear to benchmark numerical models that simulate temperature-dependent bolt shear behavior (Sarraj 2007). The connections tested were full-scale connections rather than lap-splice joints and were designed and constructed with typical European building materials to the governing codes at the time. Each connection was loaded with a combination of shear and axial force until fracture. Yu et al. (2009) showed that the capacity of Grade 8.8 bolts controls the experimentally measured connection capacity. These tests were used to validate and benchmark the bolt shear fracture mathematical model developed by Sarraj (2007).

Hu and Engelhardt (2011) conducted similar experiments to Yu et al. (2009) using U.S. building materials. Axial force was applied to shear-tab connections at varying temperatures to measure the axial force–deformation (P – δ) relationship for bolt shear and plate bearing failure modes. Each specimen consisted of an ASTM A992 (ASTM 2015b) W12 \times 16 beam with a 9.5-mm (3/8-in.) thick shear-tab with three 19-mm (3/4-in.) ASTM A325 bolts. The tests

were conducted at ambient temperature, 400, 500, 550, and 700°C. The controlling limit state at ambient temperature was bolt bearing on the beam web. However, as the temperature increased more shear deformation of the bolts was observed after the tests. At temperatures above 500°C bolt shear fracture was the controlling limit state and little to no bolt hole deformation was observed after the test.

Hanus et al. (2011) continued to investigate the bolt shear stress behavior of Grade 8.8 bolts with temperature, performing ambient, steady-state, and real fire tests on full-scale bolted connections. Hanus et al. (2011) performed the heated tests by heating to a target temperature and allowing the temperature to stabilize for 15 min prior to loading. This stabilization phase was used to ensure the temperature of the bolt at the shear plane was the same as the temperature measured on the head of the bolt. The results of these tests demonstrated that at temperatures above 500°C the shear strength of the bolt decreases but the ductility increases.

Kodur et al. (2012) tested a series of ASTM A325 (ASTM 2014c) and ASTM A490 (ASTM 2014b) bolts at elevated temperature to investigate the thermal and mechanical properties of the bolts. Seven steady-state tests were performed at temperatures ranging from ambient temperature to 800°C. Similar to the tests performed by Hanus et al. (2011), specimens were heated to a target temperature followed by a stabilization phase for 15 min prior to loading. The results from the tests were similar to those of Hanus et al. (2011), in which with increasing temperature, the shear strength of the bolts decreases with increasing ductility. At ambient temperature, the bolts fractured with a fibrous pullout type fracture surface. However, at temperatures above 400°C the fracture surface was more cup-cone shaped and became more so as the temperature increased above 500°C. The cup-cone shape of the fracture surface of the bolts at elevated temperatures demonstrates a more ductile failure mode.

Hirashima et al. (2014) tested 16 specimens of bolted double-splice friction joints at ambient temperature, 400, 500, and 700°C. The purpose of this investigation was to quantify bolt shear and plate bearing behavior at various temperatures. Hirashima et al. (2014) examined four parameters: plate thickness, vertical end distance, pretension of the bolt, and temperature. Each specimen consisted of four plates and two bolts: two main plates, two splice plates, and two high-strength bolts. The results of these tests showed that at temperatures greater than 400°C the controlling failure mode of the lap-splice joint changed from plate bearing to bolt shear. Hirashima et al. (2014) also observed that plate thickness had the greatest influence on the overall ductility of the joint. Pretensioned bolts did not influence the connection capacity at elevated temperatures.

Previous Numerical Research

Sarraj (2007) developed simple temperature-dependent nonlinear mathematical models for axial force–deformation (P – δ) relationships for different components within the connection: (1) bolt shear fracture; (2) bolt bearing on beam web; and (3) bolt bearing on shear-tab. Yu et al. (2009) validated the model developed for bolt shear fracture through experimental tests. The initial stiffness of these mathematical models is based upon the model developed by Rex and Easterling (2003). Although the bolt shear numerical model was benchmarked by Yu et al. (2009), the plate bearing numerical axial force–deformation numerical model has not been experimentally validated. This numerical model assumes that the bolt bearing deformation increases indefinitely as the axial force on the connection increases. This is an unrealistic assumption for postpeak ductility.

Agarwal et al. (2014) modified Sarraj (2007) bolt bearing models in the postpeak behavior. Agarwal et al. (2014) modified the

declining portion of the force–deformation curve to match that of the bolt shear behavior. The modified relationship assumes to follow the original Sarraj (2007) curve until bolt bearing deformation is equal to half the diameter of the bolt and then reduces linearly to zero at a displacement equal to the bolt diameter. This force–deformation (P – δ) relationship will be compared with the force–deformation relationship experimentally measured by the authors.

Design of Experiments

The authors tested a series of lap-splice joints to measure the temperature-dependent bolt shear and plate bearing axial force–deformation (P – δ) behavior of connections. Each lap-splice joint was constructed using two ASTM A36 (ASTM 2014a) plates, connected with one ASTM A325 (ASTM 2014c) bolt. The specimens were tested in steady-state conditions at ambient temperature, 400 and 600°C. Each of these tests used high-temperature ceramic fiber heaters to heat the specimen. Both testing series used the same test setup and instrumentation.

Test Setup

The test setup for both the plate bearing and the bolt shear tests consisted of two steel beams connected by two hydraulic rams and post tensioning bars. Fig. 1 shows the loading frame and test setup along with dimensions of the bolt shear lap-splice joint specimen. The bottom beam of the loading frame was post tensioned to the laboratory floor, whereas the top beam remained vertically unrestrained. Fig. 1(a) shows an elevation view of the loading frame with a specimen. Each specimen was bolted to the top and bottom loading beam through a T-stub connection as shown in Figs. 1(b and c). Two 305 × 305 mm (12 × 12 in.) ceramic heaters with a maximum surface temperature of 1,250°C were used to heat each side of the specimen at a rate of 15°C/min. Insulation was used to protect the sensor equipment and the loading frame from heat damage.

Instrumentation

Bolt and plate displacements were measured using voltage sensors. Displacement transducers and string potentiometers were attached to metal strips welded to each location shown in Fig. 2(a). In Fig. 2(a), SP designates the location of each string potentiometer used within the setup. The displacement transducers used that were not string potentiometers were simple displacement transducers.

Two displacement sensors were used at each welded strip to account for potential rotation of the upper loading beam within the test frame during each test. The displacement measurements from these two sensors were averaged. For example, the average of SP1 and SP2 was the measured displacement of the bolt head. Likewise, the average of SP7 and SP8 was the measured displacement of the end of the bolt shank. Bolt shear deformation was calculated as the relative movement of the end of the bolt shank to the bolt head. The relative movement of the bolt head versus Plate 2 (lower plate) was the bolt bearing deformation for Plate 2. The relative movement of the end of the bolt shank versus Plate 1 (upper plate) was the bolt bearing deformation for Plate 1. Each displacement sensor was mounted to the lower loading beam.

The temperature distribution through the thickness of the bolt and on the face of both plates was measured using Type K thermocouples. Fig. 2(b) shows the thermocouple locations in each of the experiments. Thermocouples were mounted on both the head and tail of the bolt, and both plates of the lap-splice joint specimens. A hole with 3.2 mm (0.125 in.) diameter was drilled through the bolt from the bolt head to a location that was approximately 3.2 mm

(0.125 in.) away from the shear plane. A thermocouple was placed inside of this hole to measure the temperature near the shear plane of the bolt. The hole did not cross the shear plane of the bolt and therefore did not affect the experimentally measured bolt shear capacity.

Testing Protocol

Each specimen was tested under steady-state conditions. Heat was applied to both surfaces of the specimen. When the target temperature was reached, and the temperature near the shear plane of the bolt was approximately the same as the temperature at the head of the bolt, then loading was applied to the specimen while holding the target temperature constant. Loading was applied to each specimen at the rate of approximately 1 kip/min. The tests were terminated when failure occurred in the specimen (bolt shear fracture or tearout failure of the plate) or when the specimen could no longer carry the load applied by the hydraulic ram. This was quantified as the calculated stiffness of the specimen was approaching zero.

Bolt Shear Tests

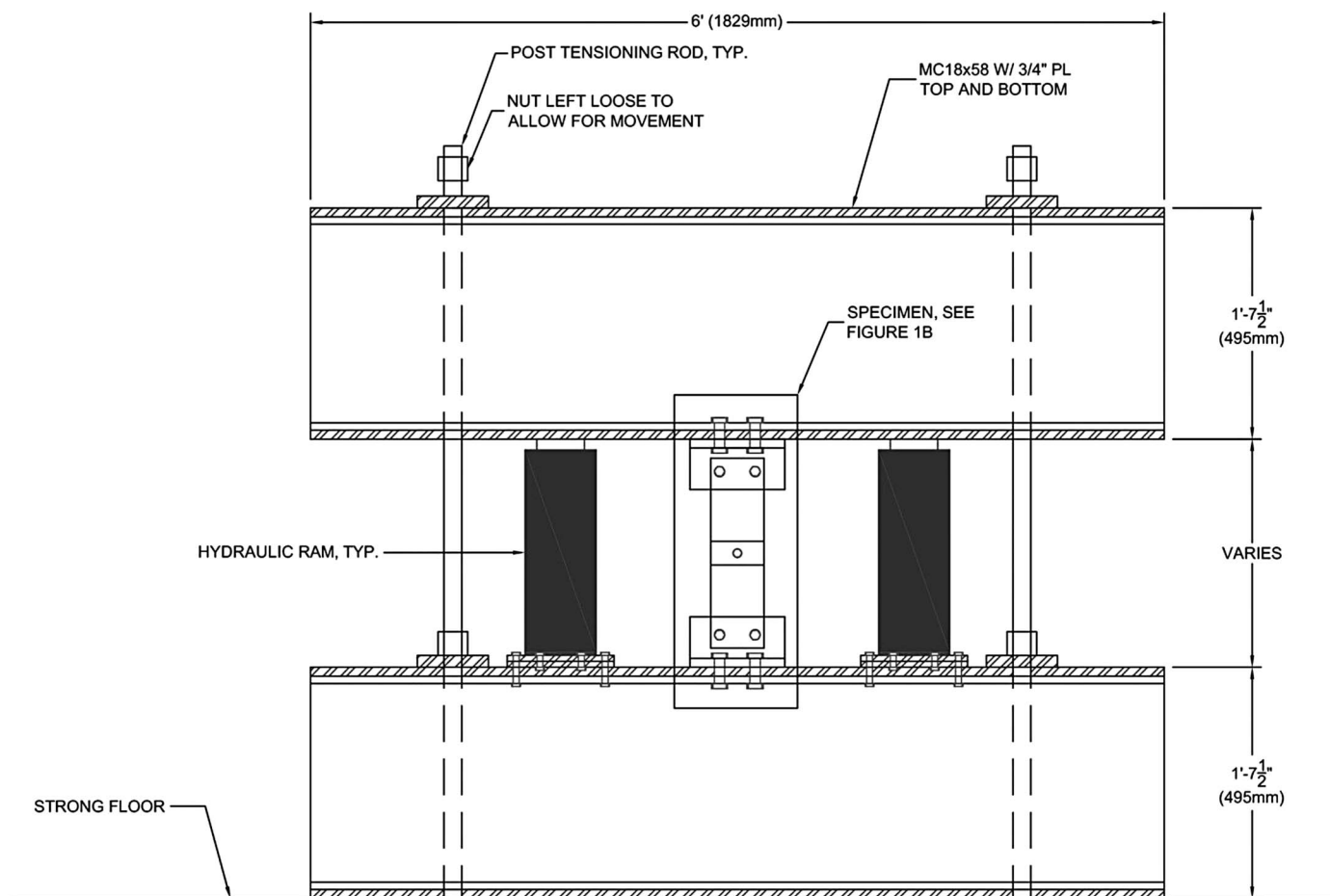
Four lap-splice joint specimens were tested to measure the temperature-dependent axial force–deformation (P – δ) relationship for bolt shear failure mode. The experimental results were compared to bolt shear tests performed by other researchers (Kirby 1995; Yu 2006; Yu et al. 2009; Hu et al. 2011; Kodur et al. 2012). Table 1 shows the testing matrix of these four specimens along with failure load (P) and failure shear displacement (δ). Each specimen consisted of an ASTM A325 bolt with 19 mm (0.75 in.) diameter connecting two ASTM A36 plates with 12.7 mm (0.5 in.) thickness. The specimens were designed such that bolt shear was the controlling limit state at ambient temperature; therefore, an edge distance of 50.8 mm (2 in.) was used in each specimen. Each specimen used ASTM F436 (ASTM 2016) washers and ASTM A563 (ASTM 2015a) Grade DH nuts.

Bolt shear fracture is typically categorized as a brittle fracture; however, at elevated temperatures the bolt shear fracture surface was observed as concave, implying a more ductile failure mode than at ambient temperature. The two specimens tested at ambient temperature fractured at measured shear displacements of 5 and 6.9 mm for BS-1 and BS-2, respectively. These two tests were used as control specimens for the heated tests. The failure load and failure displacements of these tests were within 5% of one another, providing consistency in the testing protocol, and are shown in Table 1.

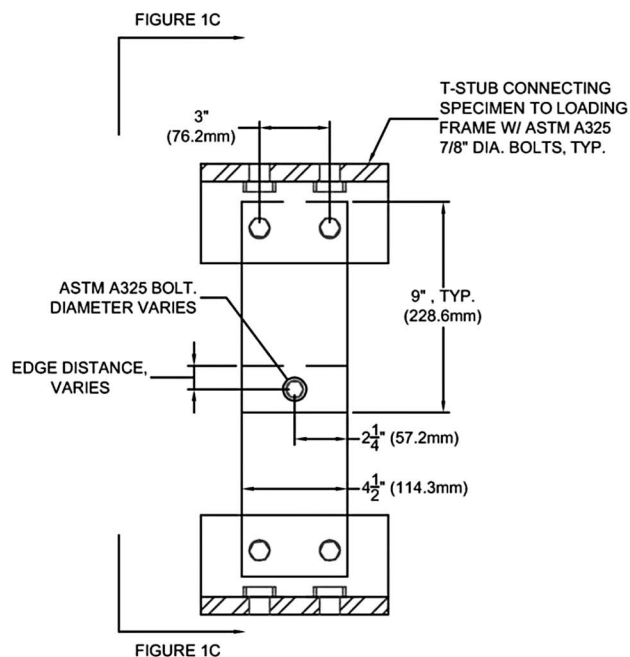
Fig. 3 shows the bolt hole of each bolt shear specimen after the completion of the tests. Limited plate bearing deformation was observed during these experiments. Photographs of the fractured bolts, including the fracture surface from test BS-1, BS-3, and BS-4 are shown in Figs. 4–6.

Failure of Specimens BS-1 and BS-2 was defined by bolt shear fracture, however, failure of BS-3 and BS-4 was defined by loss of load-carrying capacity of the specimen (stiffness of the specimen approached zero). After testing BS-3 and BS-4, the bolt was not completely fractured. The fracture surface of the bolt in Specimens BS-1 and BS-2 was shiny and smooth, but not flat. The partial fracture surface of the bolt after testing of Specimen BS-3 showed blue color and the texture was rougher than the fracture surface of the bolts in the ambient tests.

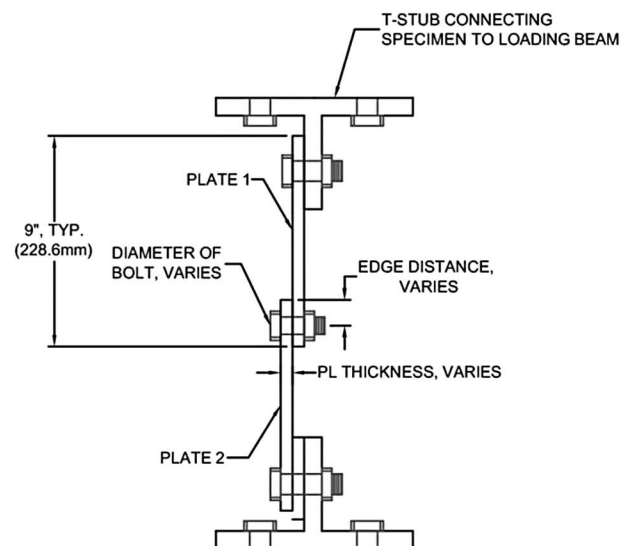
Fig. 7 shows the experimentally measured axial force–deformation (P – δ) data for all the tests. The initial linear portion of the curve represents the shear stiffness of the bolt. As the temperature increased, the measured shear stiffness and strength of the bolts decreased. The shear displacement of the bolt increased with



(a)



(b)



(c)

Fig. 1. Testing frame for bolt shear and plate bearing lap-splice joint: (a) elevation view of test setup; (b) elevation view of specimen dimensions and setup; (c) profile view of specimen setup

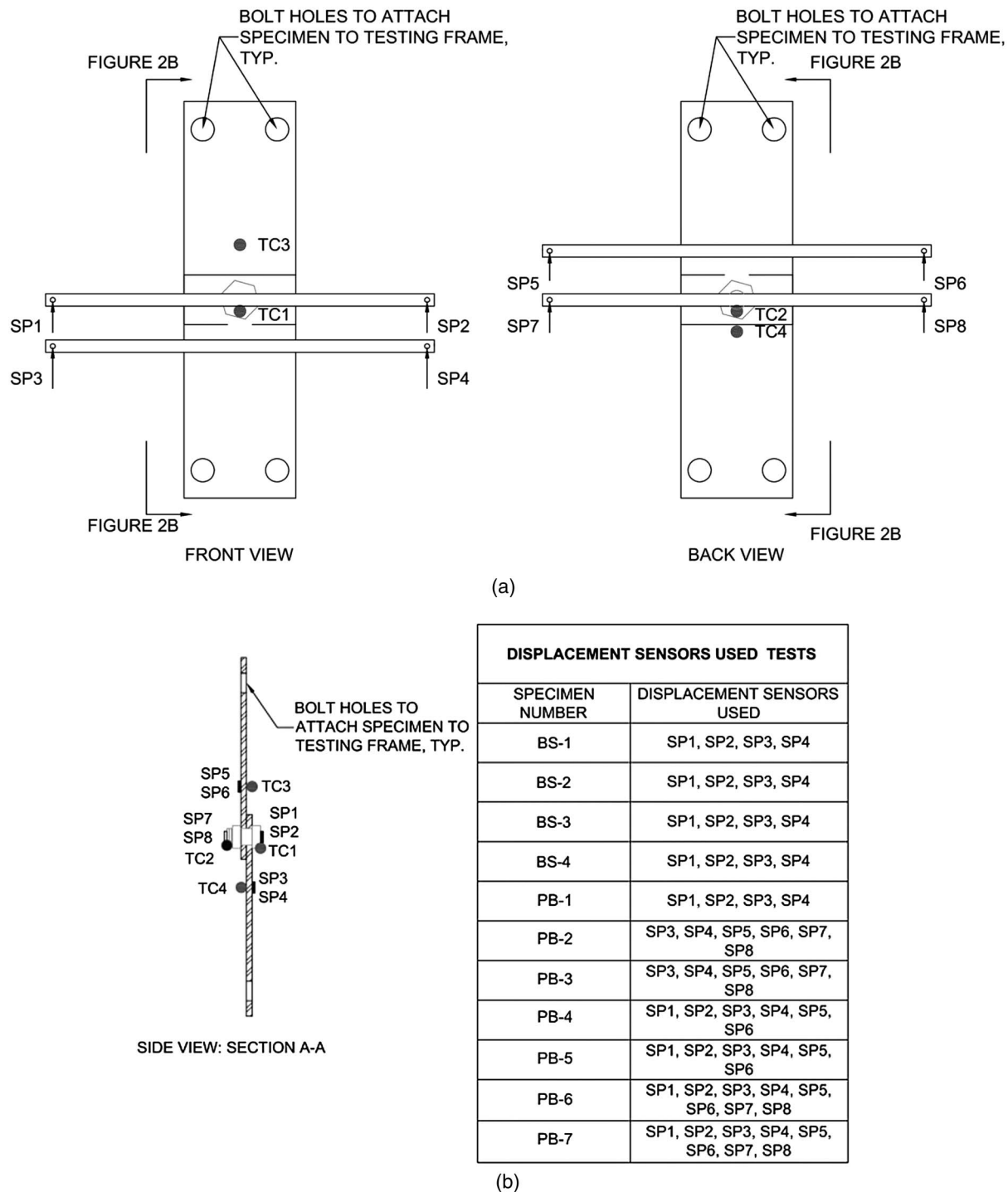


Fig. 2. Instrumentation layout for lap-splice joint tests: both bolt shear and plate bearing: (a) elevation view of instrumentation; (b) profile view of instrumentation layout and string potentiometers used in each experiment

Table 1. Test Matrix and Results for Lap-Splice Joints Tested for Bolt Shear Failure

Specimen name	Temperature	Failure load, P [kN (kip)]	Failure axial displacement, δ [mm (in.)]
BS-1	Ambient	137 (30.8)	5 (0.2)
BS-2	Ambient	133 (29.9)	6.9 (0.27)
BS-3	400°C	102 (22.9)	10.7 (0.42)
BS-4	600°C	43 (9.7)	10.9 (0.43)

increasing temperature, implying increasing ductility. The shear strength of the bolt and failure displacement are listed in Table 1. The retention factors for each of the bolts are shown in Fig. 8.

Fig. 8 compares the results of these experiments with the results of bolt shear tests performed by other researchers (Kirby 1995; Yu 2006; Yu et al. 2009; Hu et al. 2011; Kodur et al. 2012). The retention factors are defined as the measured bolt shear capacity at designated temperature divided by the bolt shear capacity at ambient temperature. Fig. 8 shows the comparison between the experimentally obtained retention factors and the calculated retention

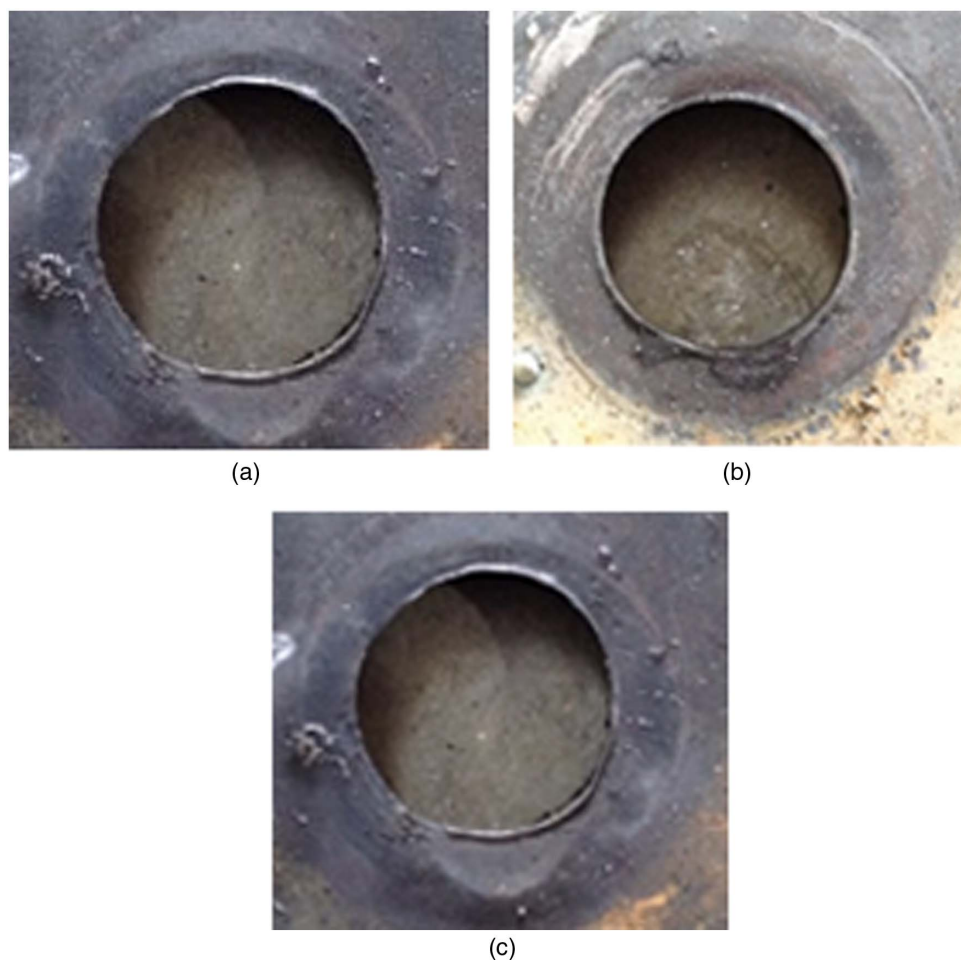


Fig. 3. Bolt hole after each bolt shear test: (a) BS-1 (ambient temperature); (b) BS-3 (400°C); (c) BS-4 (600°C)



Fig. 4. Bolt shear fracture for Specimen BS-1 (ambient temperature): (a) profile view or shear fracture of bolt; (b) fracture surface of bolt after experiment

factors per Eurocode 3. Fig. 8 shows that the retention factors obtained from the tests described in this paper are consistent with those obtained by other researchers.

Plate Bearing Tests

Seven single-bolted lap-splice joints were tested at elevated temperatures to investigate the temperature-dependent plate bearing (tearout) failure mode. Geometric parameters of the plates were varied to quantify their influence on the temperature-dependent plate bearing capacity. The testing parameters included (1) temperature,

(2) bolt diameter, and (3) plate thickness. The experimentally obtained axial load–deformation (P – δ) relationships were compared with the numerical model developed by Sarraj (2007) and further refined by Agarwal et al. (2014).

Each specimen was tested under steady-state conditions in which the specimen was heated to a target temperature, and then loaded to failure while the temperature remained constant. Failure of the specimen was categorized as either tearout failure of the plate or loss of load-carrying capacity of the specimen. The testing matrix, maximum axial forces (P), and maximum plate deformation (δ) are shown in Table 2.



Fig. 5. Bolt shear fracture for Specimen BS-3 (400°C): (a) profile view of shear fracture of bolt; (b) fracture surface of bolt after experiment



Fig. 6. Bolt shear fracture for Specimen BS-4 (600°C): (a) profile view of shear fracture of bolt; (b) fracture surface of bolt after experiment

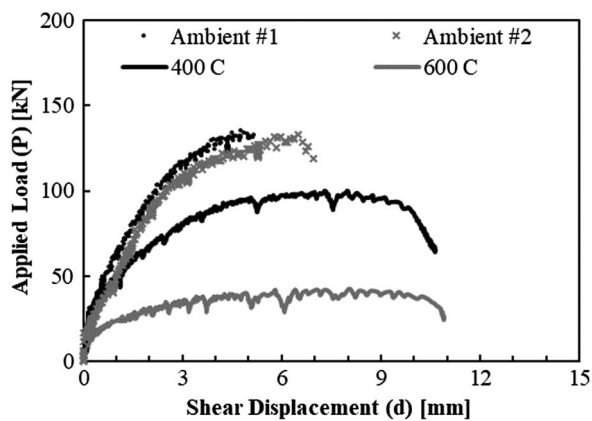


Fig. 7. Applied load–axial displacement (P – δ) for bolt shear lap-splice joint tests

The plates in the specimens presented in Table 2 were designed with standard bolt holes with minimum required edge distances prescribed by the AISC *Specification* [AISC 360-16 (AISC 2016)]. All steel plates had widths of 114 mm (4.5 in.). The yield and tensile strengths of the plates were determined through coupon tests and are summarized in Table 3. The bolts in all the tests were snug-tight, and the washer was installed on the side of the nut. The estimated plate bearing strength and bolt shear strength of the specimens were calculated using AISC Equations J3-6b and J4-4 [AISC 360-10 (AISC 2010)]. The retention factors

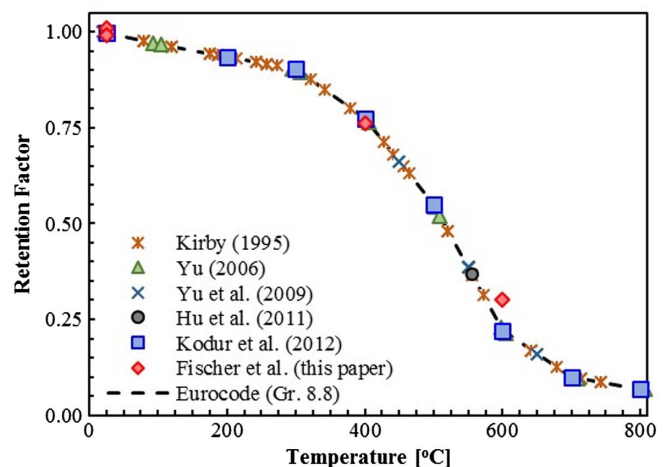


Fig. 8. Experimentally measured retention factors for ultimate bolt stress varying with temperature compared with Eurocode 3

for the tensile strength of the plates were assumed to comply with the retention factors developed by NIST researchers and presented in NIST (2009). The retention factors for the bolt ultimate stress were assumed to follow the AISC *Specification* (AISC 360-16).

The two plates in the specimen are referred to as Plates 1 and 2. Plate 1 is connected to the bottom beam of the loading frame, and Plate 2 is connected to the top beam of the loading frame. Bearing

Table 2. Test Matrix and Results for Lap-Splice Joints Tested for Plate Bearing Failure

Specimen name	Temperature (°C)	Bolt diameter [mm (in.)]	Plate thickness [mm (in.)]	Failure load, P [kN (kip)]	Failure axial displacement, δ [mm (in.)]
PB-1	Ambient	19 (0.75)	6.35 (0.25)	77.4 (17.4)	5.6 (0.22)
PB-2	402	19 (0.75)	6.35 (0.25)	64.4 (14.5)	22.9 (0.9)
PB-3	610	19 (0.75)	6.35 (0.25)	30.5 (6.9)	38.8 (1.5)
PB-4	406	22.2 (0.875)	6.35 (0.25)	76.2 (17.1)	27.2 (1.1)
PB-5	605	22.2 (0.875)	6.35 (0.25)	33 (7.4)	25.8 (1)
PB-6	417	19 (0.75)	9.5 (0.375)	100.6 (22.6)	57.1 (2.2)
PB-7	607	19 (0.75)	9.5 (0.375)	46.1 (10.4)	29.9 (1.2)

Table 3. Measured Material Properties of Plates Used for Lap-Splice Joints Tested in Plate Bearing

Thickness of plate [mm (in.)]	Yield stress [MPa (ksi)]	Ultimate stress [MPa (ksi)]
6.4 (0.25)	265 (38.4)	401 (58.2)
9.53 (0.375)	288 (44.1)	328 (50.3)

failure of Plate 2 was observed prior to Plate 1. Bolt rotation was observed while testing Specimens PB-2 and PB-3. The bolt rotation occurred because of double curvature in the lap-splice joint. This bolt rotation can skew the experimental data collected. To minimize the influence of bolt rotation on the measured axial force–deformation (P – δ) relationship, additional displacement sensors were added to subtract this rotation out of the data collected. The measurements are corrected based on the assumption that the bolt is rotating with rigid body movement about the shear plane of the bolt. Using the length of the bolt on either side of the shear plane and the displacements of the bolt head and tail, the rotation of the bolt throughout the test, and the resulting displacement of the bolt head and tail due to this rotation, can be calculated. Fig. 9 shows the bolt rotation and double curvature observed after testing PB-2. Double curvature of the plates was also observed after testing Specimens PB-3, PB-4, PB-5, and PB-6.

Figs. 10–12 show each bolt bearing specimen after the completion of the test. Additional photos have been compiled and are available in (Zhu et al. 2014). The photos in Figs. 10–12 show large bolt hole elongation observed in Specimens PB-1, PB-2, PB-3, PB-4, and PB-5. These specimens used plates with 6.4 mm (0.25 in.) thickness. Specimens PB-6 and PB-7 used plates with 9.5 mm (0.375 in.) thickness, and limited bolt hole elongation was observed after the testing of these specimens.

Figs. 13(a–c) show the applied axial load to the specimen (P) versus the plate deformation (δ) of each of the plates. The test data is compared to the predicted plate bearing axial force–deformation (P – δ) using the component model (Sarraj 2007; Agarwal et al. 2014). The bolt bearing deformation of Plate 1 shown in Figs. 13(a–c) was calculated as the difference in the measured deformation of Plate 1 and the bolt head. Likewise, the bolt bearing deformation of Plate 2 was calculated as the difference in the measured displacement of Plate 2 and the bolt nut. The photos of the plates after the experiments show that the deformation of the plates was not symmetrical. Plate 2 controlled the failure of the control Specimen (PB-1) and the specimens tested at 400°C, whereas Plate 1 controlled the failure of the specimens tested at 600°C regardless of plate thickness and bolt diameter. As discussed previously, displacement of the plates, bolt head, and bolt nut were considered during the experiments.

**Fig. 9.** Cross section through lap-splice joint of Specimen 2-PB-400

Additional displacement sensors were used to measure the rotation of the bolt while testing Specimens PB-5, PB-6, and PB-7. This data was used to remove the effects of bolt rotation from the applied load–deformation (P – δ). The applied load–deformation (P – δ) data for Specimen PB-6 is shown in Fig. 14. This data is shown corrected and uncorrected for the out-of-plane bolt rotation. This figure shows there is no significant difference between the two. The relationships shown in Figs. 13(a–c) are corrected for the bolt rotation.

Test Results

Specimen PB-1 used two 6.4 mm (0.25 in.) steel plates connected with one bolt with diameter of 19 mm (0.75 in.). The failure mode of this specimen was tearout failure of Plate 2. Figs. 10(a and b) show fracture on one side of the bolt hole of Plate 2 of Specimen PB-1. The fracture is parallel to the direction of loading in the specimen. Limited bolt shear deformation was observed after the test. The axial force–deformation (P – δ) for Specimen PB-1 is shown in Fig. 13(a). The test results show the tearout fracture limit state was a sudden fracture at peak load.

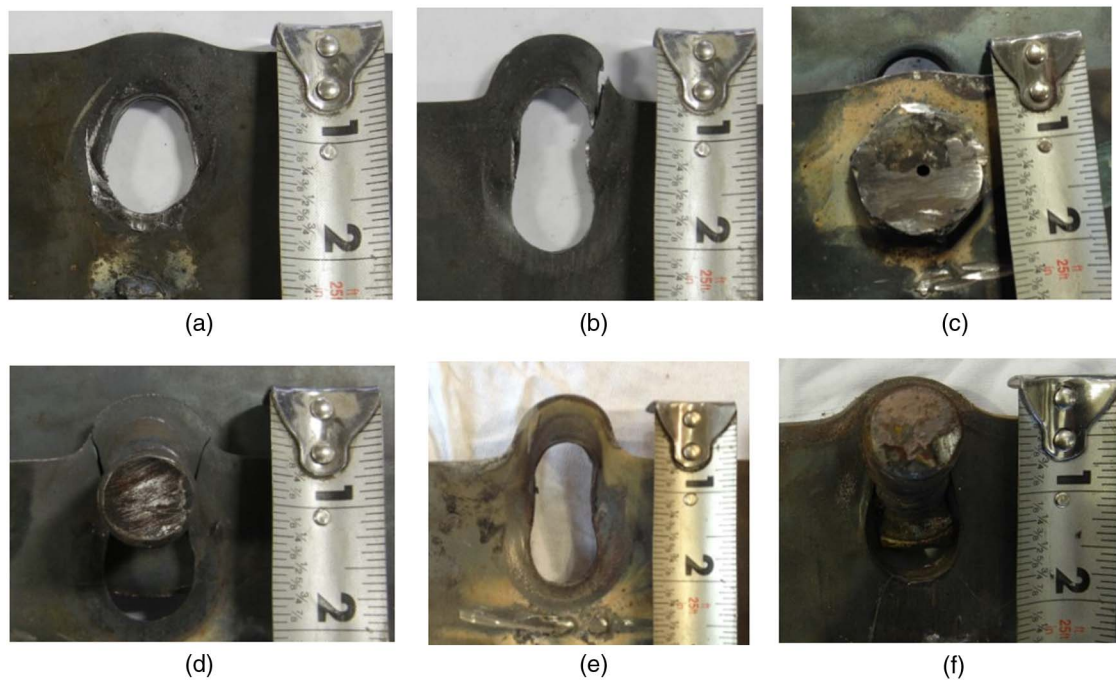


Fig. 10. Lap-splice joints after testing for plate bearing failure mode: (a) Specimen PB-1, Plate 1; (b) Specimen PB-1, Plate 2; (c) Specimen PB-2, Plate 1; (d) Specimen PB-2, Plate 2; (e) Specimen PB-3, Plate 1; (f) Specimen PB-3, Plate 2

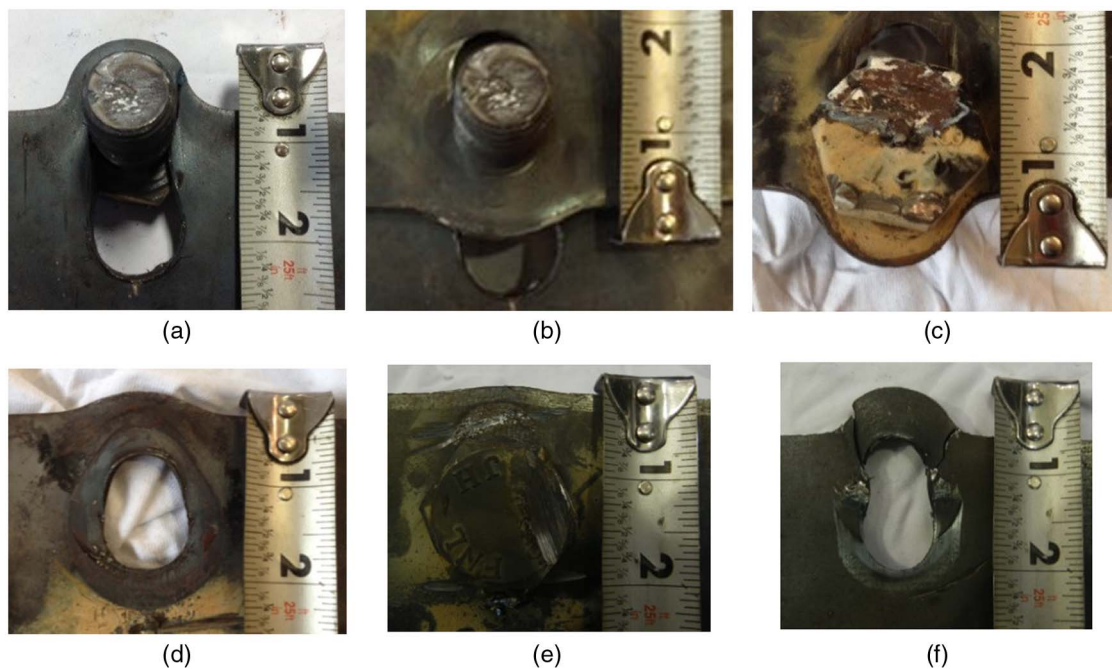


Fig. 11. Lap-splice joints after testing for plate bearing failure mode: (a) Specimen PB-4, Plate 1; (b) Specimen PB-4, Plate 2; (c) Specimen PB-5, Plate 1; (d) Specimen PB-5, Plate 2; (e) Specimen PB-4, Plate 1; (f) Specimen PB-6, Plate 2

Specimens PB-2 and PB-3 used the same size plates and bolt as Specimen PB-1, but varied the temperature of testing to 400°C and 600°C, respectively. Specimen PB-2 failed in tearout failure of the bolt hole in Plate 2. The fracture path was flared, and fracture occurred on both sides of the bolt hole. This fracture is shown in Figs. 11(b and d). The retention factor from Eurocode 3 for the steel plate ($k_{y,T}$) at 400°C is 1.0; however, the maximum measured load capacity (P_m) of the lap-splice joint was reduced by 20% from

Specimen PB-1. The measured applied load–deformation (P – δ) for Specimen PB-2 is shown in Fig. 13(a). Similar to Specimen PB-1, there is a sudden drop in load-carrying capacity after the tearout fracture of the plate.

The test of Specimen PB-3 was stopped when the deformation of the plate exceeded 1.5 times the diameter of the bolt (d_b). Because of this criterion, the test was stopped before tearout failure of the plates. Whereas bolt shear deformation was not observed

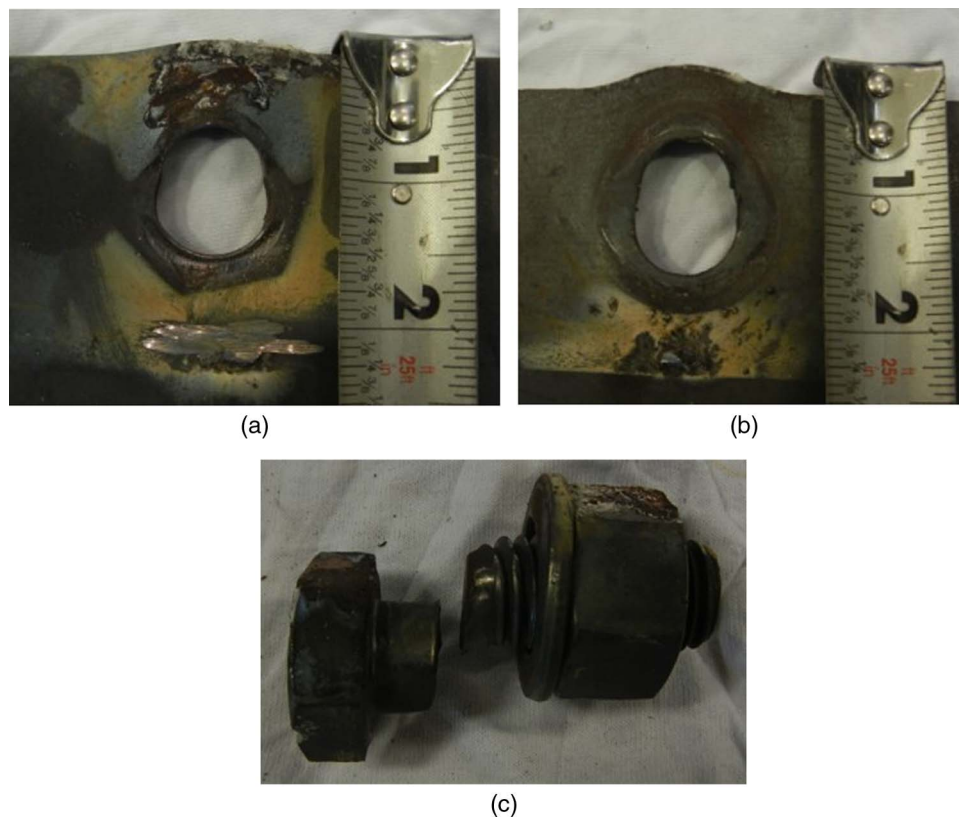


Fig. 12. Specimen PB-7 lap-splice joint: (a) Plate 1; (b) Plate 2; (c) bolt shear fracture

within Specimen PB-2, it was observed after testing Specimen PB-3. The retention factor from Eurocode 3 for the steel plate ($k_{y,T}$) at 600°C is 0.47. The maximum measured load capacity (P_m) of Specimen PB-3 was 60% of that of Specimen PB-1. The measured axial load–deformation (P – δ) relationship data is shown in Fig. 13(a). Figs. 10(e and f) show the specimen after testing. Compared with Specimens PB-1 and PB-2, the bolt hole elongation increased during the testing of Specimen PB-3.

Specimens PB-4 and PB-5 used plates with 6.4 mm (0.25 in.) thickness connected with one bolt having a diameter of 22.2 mm (0.875 in.). Failure of Specimen PB-4 was controlled by tearout failure of Plate 1. Fracture occurred only on one side of the bolt hole and, similar to Specimen PB-2, the fracture was flared rather than parallel with the direction of loading. No visible bolt shear deformation was observed after the test. Increasing the diameter of the bolt increased the maximum measured load capacity (P_m) by 18% from Specimen PB-2. The measured applied load–axial displacement (P – δ) is plotted in Fig. 13(b). Figs. 11(a and b) show Specimen PB-4 after the experiment was complete. The figures show that the bolt hole elongation of Specimen PB-4 is much larger than the bolt hole elongation observed after testing PB-2.

Specimen PB-5 used the same geometry of PB-5; however, the experiment was performed at 600°C. Similar to testing of PB-3, the test was stopped when the plate deformation exceeded 1.5 times the diameter of the bolt (d_b). Whereas bolt shear deformation was observed after testing PB-3, no bolt shear deformation was observed when the bolt diameter was increased to 22.2 mm (0.875 in.). The maximum measured load capacity (P_m) increased by 4% from Specimen PB-3, which is small when variations in fabrication and construction of the specimen are considered. Figs. 11(c and d) show Specimen PB-5 after failure. The bolt hole

elongation is approximately the same as the bolt hole elongation observed in Specimen PB-3. The applied load–axial displacement (P – δ) is shown in Fig. 13(b).

Specimens PB-6 and PB-7 used plates with 9.5 mm (0.375 in.) thickness connected with one bolt having a 19 mm (0.75 in.) diameter. Specimen PB-6 failed because of tearout failure of Plate 1. Similar to Specimen PB-2, the fracture occurred on both sides of the bolt hole in a flared path and is shown in Figs. 11(e and f). No bolt shear deformation was observed after this test. An increase in plate thickness from 6.4 to 9.5 mm increased the maximum measured load capacity (P_m) by 56%. The measured applied load–deformation (P – δ) data is shown in Fig. 13(c).

Specimen PB-7 used the same geometry as Specimen PB-6 and was tested at 600°C rather than 400°C. The test was stopped when bolt shear fracture occurred. Fig. 13 shows the bolt shear fracture and plates after the test. The bolt hole elongation is smaller than the other specimens tested at 600°C (PB-3 and PB-5). The increase in plate thickness from 6.4 to 9.5 mm from Specimen PB-3 increased the maximum load capacity (P_m) by approximately 50%. This is consistent with the increase between Specimens PB-2 and PB-6. The measured applied load–axial displacement (P – δ) data is shown in Fig. 13(c).

Comparison of Test Data with Numerical Models

Hirashima et al. (2014) showed good comparison between their plate bearing testing data and the component model developed by Sarraj (2007). The specimens used either 9- or 19-mm plates for the lap-splice joint, and one 20-mm-diameter bolt. In all of the cases, the measured load-carrying capacity of the lap-splice joint was larger than the plate bearing capacity predicted by the component model (Hirashima et al. 2014).

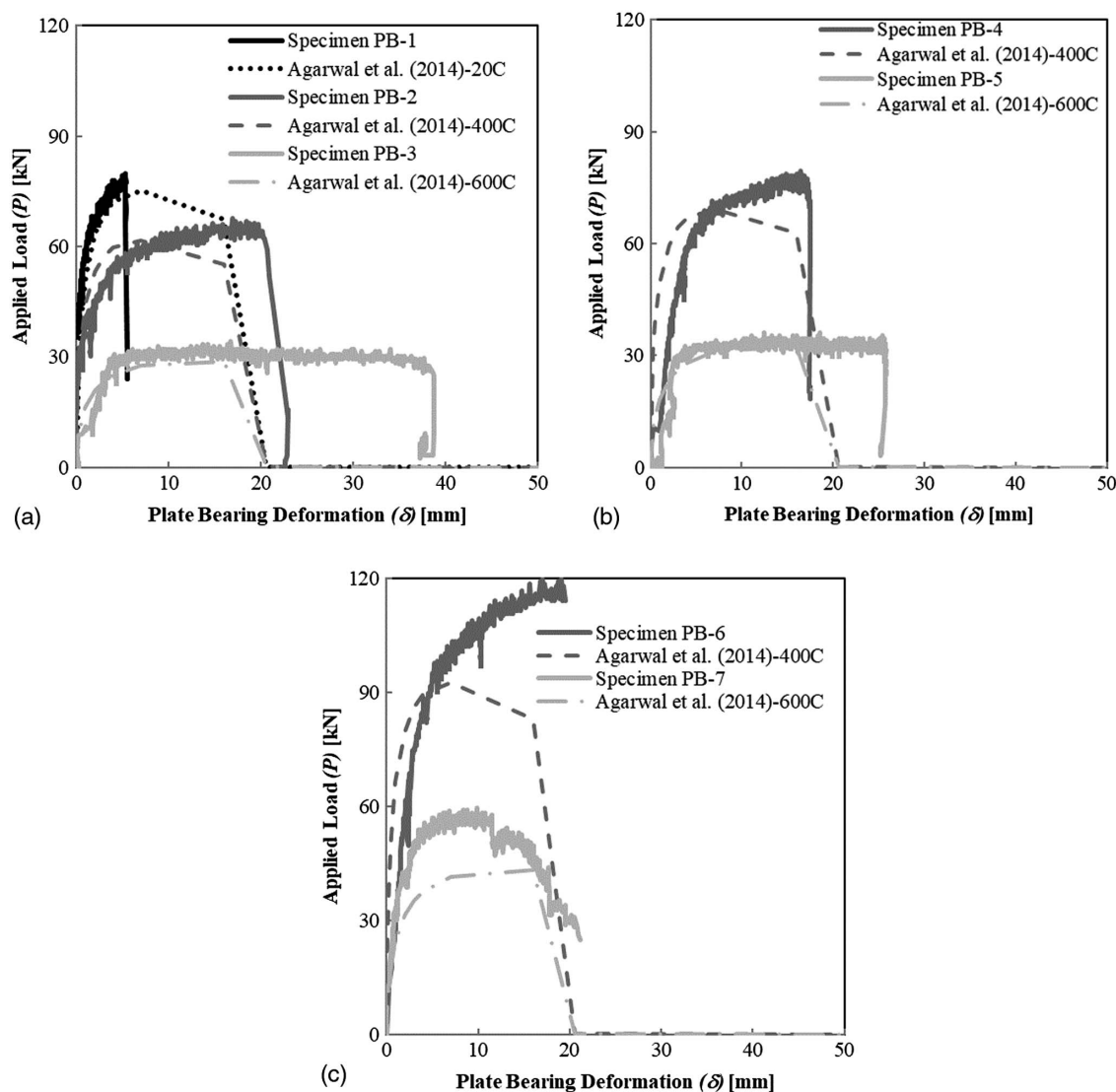


Fig. 13. Applied load–axial displacement (P – δ) for lap-splice joints tested for plate bearing failure modes compared with component model developed by Sarraj (2007) and Agarwal et al. (2014): (a) Specimens PB-1, PB-2, and PB-3; (b) Specimens PB-4 and PB-5; (c) Specimens PB-6 and PB-7

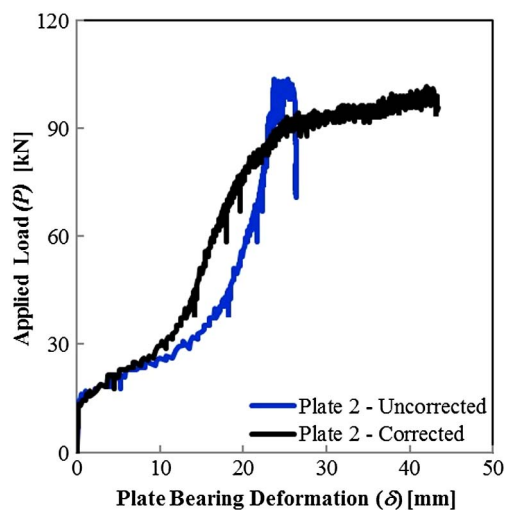


Fig. 14. Comparison of corrected and uncorrected axial load–axial deformation for PB-5

The test results presented in this paper showed that when a 6.4 mm plate was used in the lap-splice joint, the numerical model shows good agreement with the test data as the applied load increases. However, as shown in the test data, the tearout fracture limit state was a sudden fracture at peak load. This sudden fracture is not reflected in the component model (Sarraj 2007; Agarwal et al. 2014). Rather the component model shows a gradual decrease in load-carrying capacity of the lap-splice joint after peak applied load. This difference can be seen in Fig. 13(a) for Specimens PB-1 and PB-2.

The test results demonstrated that for specimens tested at 600°C, there is more ductility within the specimen than the numerical component model (Sarraj 2007; Agarwal et al. 2014) considers. The failure displacement of Specimens PB-3 and PB-5 are larger than predicted by the component model because there was both bolt shear and plate bearing deformation in the specimen. Figs. 13(a and b) show the comparison between the numerical component model and the measured axial load–deformation behavior of the lap-splice joint.

The test results demonstrated that for specimens tested using plates with 9.5 mm (0.375 in.) thickness, the numerical component

model (Sarraj 2007; Agarwal et al. 2014) underestimates the maximum axial load-carrying capacity of the lap-splice joint. Fig. 13(c) shows a comparison between the calculated and measured axial load–deformation (P – δ) relationships. For these specimens, the numerical component model is able to predict the maximum plate deformation of the specimens.

Calculated Plate Bearing Capacity

Three methods are available to calculate the bolt bearing capacity of the lap-splice joints tested. Two methods of calculating the bearing strength are from the AISC *Specification*: the 1993 *Specification* [AISC 360-93 (AISC 1993)], and the 2016 *Specification* (AISC 360-16). The third method of calculating bearing strength is from Eurocode 3. Eqs. (1)–(3) show the bearing strength as calculated by the 1993 AISC *Specification*, 2016 AISC *Specification*, and Eurocode 3. The current AISC *Specification* uses Eq. (2) to calculate bolt bearing capacity when the deformation at the bolt hole is considered during service loading conditions

$$F_{b,1} = \frac{e_2}{d_b} F_u d_b t \quad (1)$$

$$F_{b,2} = 1.2 \frac{e_2 - 0.5d_b}{d_b} F_u d_b t \quad (2)$$

$$F_{b,3} = \frac{2.5}{3} \frac{e_2}{d_b} F_u d_b t \quad (3)$$

where d_b = diameter of the bolt; e_2 = distance from the center of the bolt hole to the edge of the plate in the direction parallel to loading; F_u = ultimate stress capacity of the plates; and t = thickness of the plate.

Table 4 shows the ratio of the experimentally obtained maximum load capacity (P_m) of each specimen to Eqs. (1)–(3). The $F_{b,1}$, $F_{b,2}$, and $F_{b,3}$ bearing strengths were calculated using the geometric and material parameters of the specimens presented in Tables 2 and 3. Ultimate stress retention factors obtained from Eurocode 3 were used. The 1993 AISC *Specification* bolt bearing capacity ($F_{b,1}$) has the best correlation with the experimental data with ratios varying from 0.93 to 1.2. Both the 2016 AISC *Specification* ($F_{b,2}$) and Eurocode 3 ($F_{b,3}$) equations for bolt bearing capacity show conservative estimates for bolt bearing strength. This can be seen in Table 4 where the ratios of the experimentally measured maximum load capacity (P_m) to the calculated bolt bearing strength for $F_{b,2}$ and $F_{b,3}$ are well above 1.0 with $F_{b,2}$ being the most conservative.

Table 4. Comparison of Experimentally Measured and Calculated Bolt Bearing Capacity

Specimen name	$P_m F_{b,1}$	$P_m F_{b,2}$	$P_m F_{b,3}$
PB-1	1.2	1.60	1.44
PB-2	0.99	1.33	1.20
PB-3	1.25	1.67	1.50
PB-4	0.94	1.21	1.13
PB-5	1.09	1.39	1.30
PB-6	0.93	1.24	1.12
PB-7	1.14	1.51	1.36

Summary and Conclusions

This paper presented a discussion of the performance of simple (shear) connections during fires, specifically the plate bearing and bolt shear fracture failure modes at elevated temperatures. The authors performed and summarized a testing series that investigated the influence of various parameters (bolt diameter, plate thickness, and temperature) on these failure modes at elevated temperatures.

Experimentally measured retention factors for temperature-dependent bolt shear capacity were compared with those obtained by previous research (Kirby 1995; Yu 2006; Yu et al. 2009; Hu and Engelhardt 2011; Kodur et al. 2012) and the temperature-dependent bolt shear capacities provided in Appendix IV to the AISC *Specification* (AISC 360-16). There is good agreement between the temperature-dependent retention factors obtained by the authors and previous researchers and the AISC *Specification* (AISC 360-16).

The measured applied axial force–deformation (P – δ) relationships for plate bearing were compared with component spring models developed by Sarraj (2007). The comparison showed that the softening behavior in the component model curves was not present during the test. The tearout failure occurred suddenly, and there was little or no loss of load-carrying capacity prior to the fracture. The component model (Sarraj 2007; Agarwal et al. 2014) predicted the maximum load-carrying capacity for specimens using plates with thickness of 6.4 mm (0.25 in.). However, when the plate thickness was increased to 9.5 mm (0.375 in.), the component model (Sarraj 2007; Agarwal et al. 2014) underpredicted the maximum load for the lap-splice specimen. The component model also underpredicted the maximum axial displacement for specimens tested at 600°C using plates with thickness of 6.4 mm (0.25 in.).

Double curvature of the lap-splice specimens was observed after many of the tests. This curvature caused rotation of the bolt and may have skewed the test data for test setups that did not consider or explicitly measure this behavior. These conclusions are made from a limited number of tests performed by the authors and comparisons with previous research (Hirashima et al. 2014). Future lap-splice tests performed to evaluate the axial load–deformation relationships should be designed to limit the curvature of the plates and subsequent rotation of the bolt.

The authors found the current code level bolt bearing capacity (AISC 360-16) is conservative compared with the test results for temperature-dependent bolt bearing capacity of lap-splice joints. This conservatism is regardless of bolt diameter or plate thickness. This conservatism is acceptable because of the variability of material properties at elevated temperature, and the importance of connections in the overall stability of steel-frame buildings during fires.

The authors have summarized experimental investigations of lap-splice joints tested at elevated temperatures. These investigations have produced a wealth of information regarding failure modes and experimental data that can be used to improve the numerical component models available to designers to simulate the behavior of simple bolted connections at elevated temperatures.

References

- Agarwal, A., Selden, K. L., and Varma, A. H. (2014). “Stability behavior of steel building structures in fire conditions: Role of composite floor systems with shear-tab connections.” *J. Struct. Fire Eng.*, 5(2), 77–96.
- AISC. (1993). “Specification for structural steel buildings.” *ANSI/AISC 360-10*, Chicago.

- AISC. (2010). "Specification for structural steel buildings." *ANSI/AISC 360-10*, Chicago.
- AISC. (2016). "Specification for structural steel buildings." *ANSI/AISC 360-10*, Chicago.
- ASTM. (2014a). "Standard specification for carbon structural steel." *ASTM A36/A36M-14*, West Conshohocken, PA.
- ASTM. (2014b). "Standard specification for structural bolts, alloy steel, heat treated, 150 ksi minimum tensile strength." *ASTM A490-14a*, West Conshohocken, PA.
- ASTM. (2014c). "Standard specification for structural bolts, steel, heat treated, 120/105 ksi minimum tensile strength." *ASTM A325-14*, West Conshohocken, PA.
- ASTM. (2015a). "Standard specification for carbon and alloy steel nuts." *ASTM A563-15*, West Conshohocken, PA.
- ASTM. (2015b). "Standard specification for structural steel shapes." *ASTM A992/A992M-11*, West Conshohocken, PA.
- ASTM. (2016). "Standard specification for hardened steel washers inch and metric dimensions." *ASTM F436/F436M-16*, West Conshohocken, PA.
- Block, F. M., Burgess, I. W., Davison, J. B., and Plank, R. J. (2007). "The development of a component-based connection element for endplate connections in fire." *Fire Saf. J.*, 42(6), 498–506.
- BSCA (British Construction Steelwork Association). (2001). "Structural use of steelwork in building, code of practice for design, rolled and welded sections." *BS 5950-1: 2000*, London.
- CEN (European Committee for Standardization). (2005). "Design of steel structures. 1.2: General rules—Structural fire design." *Eurocode 3*, Geneva.
- Fischer, E. C., Selden, K. L., and Varma, A. H. (2016). "Experimental evaluation of fire performance of simple (shear) connections." *J. Struct. Eng.*, 10.1061/(ASCE)ST.1943-541X.0001664, 04016181.
- Fischer, E. C., and Varma, A. H. (2015). "Fire behavior of composite beams with simple connections: Benchmarking of numerical models." *J. Constr. Steel Res.*, 111(Aug), 112–125.
- Hanus, F., Zilli, G., and Franssen, J. M. (2011). "Behaviour of Grade 8.8 bolts under natural fire conditions—Tests and model." *J. Constr. Steel Res.*, 67(8), 1292–1298.
- Hirashima, T., Esaki, Y., and Ando, S. (2014). "Load-deformation behavior of bolted double-splice friction joints at elevated temperature." *Proc., 8th Int. Conf. on Structures in Fire*, Tongji University Press, Shanghai, China.
- Hu, G., and Engelhardt, M. D. (2011). "Investigations of the behavior of steel single plate beam end framing connections in fire." *J. Struct. Fire Eng.*, 2(3), 195–204.
- Kirby, B. R. (1995). "The behaviour of high-strength Grade 8.8 bolts in fire." *J. Constr. Steel Res.*, 33(1), 3–38.
- Kodur, V., Kand, S., and Khaliq, W. (2012). "Effect of temperature on thermal and mechanical properties of steel bolts." *J. Mater. Civ. Eng.*, 10.1061/(ASCE)MT.1943-5533.0000445, 765–774.
- NIST. (2009). "Best practices for structural fire resistance design of concrete and steel buildings." *NISTIR 7563*, U.S. Dept. of Commerce, Washington, DC.
- Rex, C., and Easterling, W. (2003). "Behavior and modeling of a bolt bearing on a single plate." *J. Struct. Eng.*, 10.1061/(ASCE)0733-9445(2003)129:6(792), 792–800.
- Sarraj, M. (2007). "The behaviour of steel fin plate connections in fire." Ph.D. dissertation, Univ. of Sheffield, Sheffield, U.K.
- Yu, H., Burgess, I. W., Davidson, J. B., and Plank, R. J. (2009). "Experimental investigation of the behaviour of fine plate connections in fire." *J. Constr. Steel Res.*, 65(3), 723–736.
- Yu, L. (2006). "Behavior of bolted connections during and after a fire." Ph.D. dissertation, Univ. of Texas, Austin, TX.
- Zhu, Q., Fischer, E. C., and Varma, A. H. (2014). *Fire behavior of bearing bolted connections*, Purdue Univ. Research Repository, West Lafayette, IN.